J. Plasma Phys. (2025), *vol*. 91, E139 © The Author(s), 2025. Published by Cambridge University Press.
This is an Open Access article, distributed under the terms of the Creative Commons Attribution licence (https://creativecommons.org/licenses/by/4.0/), which permits unrestricted re-use, distribution and reproduction, provided the original article is properly cited. doi:10.1017/S0022377825000418

Enhanced collisional losses from a magnetic mirror using the Lenard–Bernstein collision operator

Maxwell H. Rosen[1], W. Sengupta[1], I. Ochs[1], F.I. Parra[1,2] and G.W. Hammett[2]

[1]Department of Astrophysical Sciences, Princeton University, Princeton, NJ 08540, USA
[2]Princeton Plasma Physics Laboratory, Princeton, NJ 08540, USA

Corresponding author: Maxwell H. Rosen, mhrosen@pppl.gov

(Received 20 November 2024; revision received 21 March 2025; accepted 24 March 2025)

Collisions are crucial in governing particle and energy transport in plasmas confined in a magnetic mirror trap. Modern gyrokinetic codes model transport in magnetic mirrors, but some use approximate model collision operators. This study focuses on a Pastukhov-style method of images calculation of particle and energy confinement times using a Lenard–Bernstein model collision operator. Prior work on parallel particle and energy balances used a different Fokker–Planck plasma collision operator. The method must be extended in non-trivial ways to study the Lenard–Bernstein operator. To assess the effectiveness of our approach, we compare our results with a modern finite element solver. Our findings reveal that the particle confinement time scales as $a\exp(a^2)$ using the Lenard–Bernstein operator, in contrast to the more accurate scaling that the Coulomb collision operator would yield, $a^2\exp(a^2)$, where a^2 is approximately proportional to the ambipolar potential. We propose that codes solving for collisional losses in magnetic mirrors using the Lenard–Bernstein or Dougherty collision operator scale their collision frequency of any electrostatically confined species. This study illuminates the collision operator's intricate role in the Pastukhov-style method of images calculation of collisional confinement.

Keywords: Fusion Plasma, Plasma Confinement, Plasma Simulation

1. Introduction

Magnetic mirrors, or adiabatic traps, present a compelling avenue for plasma confinement through the deflection of particles away from high-field regions. In recent years, the resurgence of interest in mirrors as a fusion concept has been led by groundbreaking experiments at the collisional Gas Dynamic Trap Experiment (GDT) at the Budker Institute in Novosibirsk, Russia, which achieved

Downloaded from https://www.cambridge.org/core. UNIVERSIDAD AUTONOMA METROPOLITANA, on 17 Nov 2026 at 14:11:56, subject to the Cambridge Core terms of use, available at https://www.cambridge.org/core/terms. https://doi.org/10.1017/S0022377825000418

unprecedented transient electron temperatures of 900 eV, demonstrating the viability of mirrors in fusion endeavours (Bagryansky *et al.* 2015).

One of the most remarkable results from the GDT experiment is the stabilisation of axisymmetric mirrors against the well-understood interchange instability (Post & Rosenbluth 1966). Vortex confinement, for instance, has been shown to stabilise the $m = 1$ flute interchange mode, and finite Larmor radius effects can stabilise $m \geqslant 2$ (Beklemishev *et al.* 2010; Bagryansky *et al.* 2011; Beklemishev 2017; Ryutov *et al.* 2011; White, Hassam & Brizard 2018). Moreover, recent advancements in superconducting magnet technology and electron cyclotron heating (ECH) have motivated new experiments to extend the results of GDT (Fowler, Moir & Simonen 2017). One such experiment is the Wisconsin high-field axisymmetric mirror experiment (WHAM) in Madison, Wisconsin (Egedal *et al.* 2022; Endrizzi *et al.* 2023). Their new endeavour, using high-temperature superconducting (HTS) REBCO tapes and neutral beam injection (NBI), will investigate the magnetohydrodynamic (MHD) and kinetic stability of the axisymmetric mirror, extended into the collisionless regime. With these new experimental techniques and MHD stability in sight, questions arise related to particle and energy confinement in these new stable axisymmetric mirror configurations.

Parallel losses play a critical role in the confinement of particles and energy, which occur when particles scatter due to collisions across the loss cone (Berk & Chen 1988). Pastukhov (1974) laid the foundation for calculating parallel losses in a magnetic mirror with the method of images approach that this study uses. Pastukhov's insight showed that the steady-state balance among a low-energy source, Fokker–Planck collision operator and high-energy image sinks could be simplified by transforming the problem into an analogous Poisson equation, then solved using standard techniques from electromagnetism (Jackson 1999). Building on Pastukhov's insight, Najmabadi, Conn & Cohen (1984) extended the analysis by simplifying Pastukhov's variable transformations, reducing the number of approximations made, and including a higher-order correction, yielding a more refined solution. Recent advancements have been made by Ochs, Munirov & Fisch (2023), who included relativistic effects to Najmabadi's approach.

Although parallel dynamics is often the fastest time scale phenomenon in magnetised plasmas, many researchers are interested in studying the next-order perpendicular transport due to micro-stability and turbulence, which find their best answers in computer simulations that include collisions. With the recent investigations using the Gkeyll code to study high-field magnetic mirrors using the Dougherty collision operator (Francisquez *et al.* 2023), it is essential to understand the effect of this approximate collision operator on parallel collisional losses before it is extended to study perpendicular transport.

To understand the key details and trade-offs between different collision operators, we must first study a few important approximations in this context. A comprehensive description of two-particle collisions within the framework of a Fokker–Planck operator involves the so-called 'Rosenbluth potentials' (Rosenbluth *et al.* 1957). This fully fledged operator, while widely studied and implemented, poses computational and analytical challenges (Taitano *et al.* 2015). In some cases, approximations become a pragmatic necessity to render the problem computationally tractable. In this context, one widely used approximate collision operator is the Lenard–Bernstein (LBO) / Dougherty operator: a simple operator that captures the advection and diffusion responses from small-angle two-body collisions (Lenard & Bernstein 1958;

Downloaded from https://www.cambridge.org/core. UNIVERSIDAD AUTONOMA METROPOLITANA, on 17 Nov 2026 at 14:11:56, subject to the Cambridge Core terms of use, available at https://www.cambridge.org/core/terms. https://doi.org/10.1017/S0022377825000418

Dougherty 1964). The difference between the LBO and Dougherty collision operators is that the LBO has zero parallel streaming fluid flow velocity, while the Dougherty operator includes the parallel fluid flow velocity in calculating the drag, useful for cases where momentum conservation is important.

Novel work was performed using the Gkeyll code in projecting the Dougherty operator onto a discontinuous Galerkin framework with enhanced multi-species collisions for gyrokinetic and Vlasov–Maxwell simulations (Hakim *et al.* 2020; Francisquez *et al.* 2020, 2022). Owing to the Dougherty operator having eigenfunctions of Hermite polynomials, the GX code uses this simple collision operator (Mandell *et al.* 2022). The GENE-X code can simulate x-point geometry tokamak configurations, with their most rigorous collision operator being Dougherty (Ulbl *et al.* 2022, 2023). Other examples of plasma kinetic / gyrokinetic codes that have implemented such collision operators (at least as an option) include Ye *et al.* (2024), Celebre, Servidio & Valentini (2023), Hoffmann, Frei & Ricci (2023), Frei, Hoffmann & Ricci (2022), Perrone, Jorge & Ricci (2020), Loureiro *et al.* (2016), Grandgirard *et al.* (2016), Pezzi, Camporeale & Valentini (2016), Parker & Dellar (2015) and Hatch *et al.* (2013). An LBO / Dougherty collision operator with the appropriate definitions satisfies many properties of a good collision operator, such as conservation of density, momentum and energy (Francisquez *et al.* 2020). The most significant defect in this model is that the collision frequency is independent of velocity, leading to inaccurate results in the tail of the distribution function. Furthermore, the operator's isotropic diffusion coefficient makes no distinction between pitch-angle scattering and energy diffusion (Hirshman & Sigmar 1976). Some of the shortcomings of the Lenard–Bernstein / Dougherty operator are described by Knyazev, Dorf & Krasheninnikov (2023).

In this study, we build upon the method of images approach developed by Najmabadi *et al.* (1984), but with a focus on the LBO, since we consider a system with zero parallel fluid flow. Since the ambipolar potential of magnetic mirrors shifts the loss cone towards higher-energy particles, we must investigate the validity of the LBO's collisionality approximation at high energies. Following the method of images approach from Najmabadi *et al.* (1984), results show that the particle confinement time scales as $a\exp(a^2)$ using the LBO, in contrast to the scaling $a^2\exp(a^2)$ that more accurate Coulomb collision operator yields, where a^2 is proportional to the ambipolar potential. In addition, the average energy of lost particles is also modified. The error between the average energy of lost particles and our numerical solver is comparable to that in the study of Najmabadi *et al.* (1984). It is critical that a code using the LBO or Dougherty collision operator matches particle loss rates compared with an experiment to predict the correct ambipolar potential. Suggestions are made to reduce the collision frequency to match particle loss rates compared with the results of Najmabadi *et al.* (1984).

It is of interest to mention and discuss an alternative to the method of images approach, as the historical journey towards accurate ambipolar estimates encompasses diverse approaches. Chernin & Rosenbluth (1978) introduced an alternative derivation that approximates the loss cone as a square in velocity space, yielding insights using a linearised Fokker–Planck equation and the associated variational principle. Cohen *et al.* (1978) showed that the techniques of Chernin & Rosenbluth (1978) lacked robustness compared with Pastukhov's technique, and higher-order approximations were needed. Subsequent work by Catto & Bernstein (1981), followed by Catto & Li (1985) and Fyfe *et al.* (1981), refined this approach by eliminating the square loss cone approximation and extending the approach to

Downloaded from https://www.cambridge.org/core. UNIVERSIDAD AUTONOMA METROPOLITANA, on 17 Nov 2026 at 14:11:56, subject to the Cambridge Core terms of use, available at https://www.cambridge.org/core/terms. https://doi.org/10.1017/S0022377825000418

higher order. Catto's studies circumvent the need for an accurate solution for the distribution function by transforming the problem into parallel and perpendicular coordinates to the loss cone and then employing variational techniques to yield improved confinement times. Khudik (1997) demonstrated the comparable accuracy of fourth-order extensions of Catto's methods to Najmabadi's approach. Furthermore, these variational methods generalise to arbitrary mirror ratios and, therefore, would be more suitable for application to toroidal confinement devices, which have order unity mirror ratios. Extending these models to the LBO would not be trivial because these methods are finely tuned to the Coulomb operator. Although these methods have many good properties, we are ultimately interested in large mirror ratios, and the flexibility of variational techniques is unnecessary.

Subsequent sections will use the method of images approach to explore how the LBO collision operator changes the parallel losses of a magnetic mirror. In § 2, the problem is presented and solved systematically for the confinement time and energy loss rate. A correction factor is evaluated numerically in § 3. Results are compared with the numerical code presented in § 3. This approach's validity and applicability to mirror simulation codes are discussed in § 4. Suggestions are made for modifying the collision frequency to obtain the appropriate ambipolar potential. Finally, we conclude in § 5.

2. Method of images solution

Our solution follows closely with the methods of Najmabadi *et al.* (1984) with some key differences. In a single-particle picture of a magnetic mirror, the parallel dynamics of particle losses depend on whether they possess sufficient energy to overcome the confining forces. These forces arise from gradients in the magnetic field magnitude ($\vec{\nabla} B$) and an electrostatic ambipolar potential ($z_s e\phi$), where e is the elementary charge and z_s is the charge number of species s. When particles have enough energy to overcome the $\vec{\nabla} B$ forces in the absence of an ambipolar potential, they reside within a specific region in phase space known as the 'loss cone'. The introduction of an ambipolar potential alters the minimum energy required for escape, thereby transforming the loss cone into a 'loss hyperboloid'. The loss hyperboloid can be expressed as

$$1 - \mu^2 = \frac{1}{R}\left(1 - \frac{v_0^2}{v^2}\right). \tag{2.1}$$

Here, $\mu = \cos\theta = v_{||}/v$ is the cosine of the pitch angle, v is the total velocity $|\vec{v}|$, $v_{||} = \left(\vec{v}\cdot\vec{B}\right)/B$ is the component of the velocity parallel to the magnetic field, R is the ratio of the maximum magnetic field to the minimum magnetic field B_{max}/B_{min} and v_0 is the loss velocity corresponding to the ambipolar potential ($m_s v_0^2/2 = z_s e\phi$), where m_s is mass. The goal is to recreate this boundary, where the distribution function is null, with image sources and sinks. A model of the loss hyperboloid, source and image sinks in the problem is shown in figure 1. A source is placed at a low velocity, in a steady-state balance with the collision operator, while sinks are placed in the loss region and f_s is extended. With these sinks, the equation for f_s near the loss hyperboloid is

$$\mathcal{L}(f_s) + Q(v, \mu) = 0. \tag{2.2}$$

Downloaded from https://www.cambridge.org/core. UNIVERSIDAD AUTONOMA METROPOLITANA, on 17 Nov 2026 at 14:11:56, subject to the Cambridge Core terms of use, available at https://www.cambridge.org/core/terms. https://doi.org/10.1017/S0022377825000418

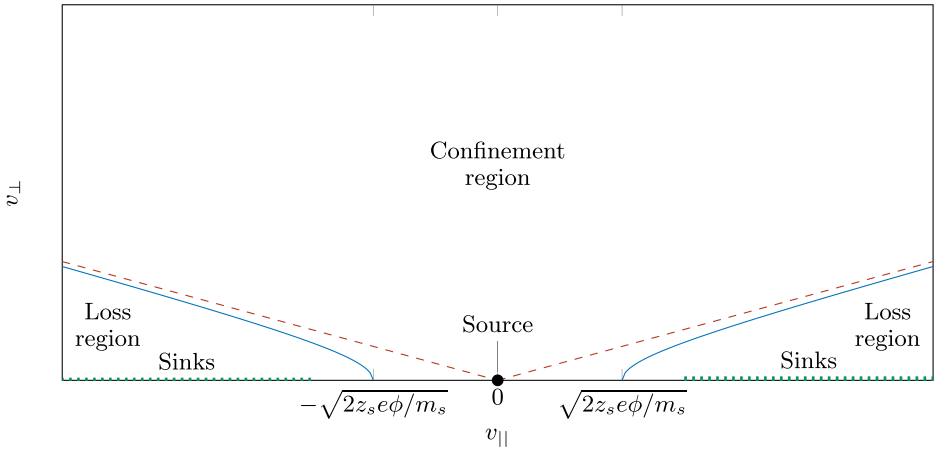


FIGURE 1. Loss boundary in velocity space for electrostatically confined particles in a magnetic mirror field. Imposed on the figure is a model depiction of the low energy source. The dotted green line represents the sinks used to solve for the distribution function. The blue line is the loss hyperboloid described in (2.1), and the red dashed line is the loss cone without an ambipolar potential.

Here, $\mathcal{L}(f_s)$ is a collision operator, which acts on the distribution function f_s of species s, and $Q(v, \mu)$ is an image sink of particles placed inside the loss region, where f_s is extended. The sink Q will be chosen to make $f_s = 0$ at the loss hyperboloid's vertex defined by (2.1) as well as have the contour of $f_s = 0$ match the radii of curvature of the loss hyperboloid at the vertex. Thus, the boundary conditions on f_s are defined as

$$f_s(v, \mu)|_{v=v_0,\mu=\pm1} = 0, \qquad \left.\frac{\partial_v f_s}{\partial_\mu f_s}\right|_{v=v_0,\mu=\pm1} = \frac{1}{Rv_0}. \tag{2.3}$$

For small v, we assume that f_s is a Maxwellian,

$$f_s(v, \mu)|_{v\to0} \to \frac{n_s}{\pi^{3/2} v_{th,s}^2} \exp(-\frac{v^2}{v_{th,s}^2}), \tag{2.4}$$

where n_s is number density, $v_{th,s} = \sqrt{2T_s/m_s}$, T_s is temperature in units of energy and v is the total magnitude of the velocity $|\vec{v}|$. Assuming a square-well approximation for the magnetic field and considering that the maximum magnetic field occurs at the mirror throat, the LBO has the form (Lenard & Bernstein 1958)

$$\mathcal{L}(f_s) = \nu_{sLBO} \frac{\partial}{\partial \vec{v}} \cdot \left(\vec{v} f_s + \frac{v_{th,s}^2}{2} \frac{\partial f_s}{\partial \vec{v}} \right), \tag{2.5}$$

where ν_{sLBO} is the collision frequency used in the LBO, $\vec{v}$ is a velocity vector and $v_{th,s}$ is the thermal velocity. Generality is left in defining the collision frequency ν_{sLBO} because it may be chosen to match certain important physical quantities and rates in its specific implementation (Francisquez *et al.* 2022). For instance, one may choose the collision frequency for the LBO to match thermal equilibration rates, Braginskii

Downloaded from https://www.cambridge.org/core. UNIVERSIDAD AUTONOMA METROPOLITANA, on 17 Nov 2026 at 14:11:56, subject to the Cambridge Core terms of use, available at https://www.cambridge.org/core/terms. https://doi.org/10.1017/S0022377825000418

heat fluxes or the Spitzer resistivity. Later in this work, we will investigate choosing the LBO's collision frequency to match ambipolar collisional losses from a magnetic mirror field. To simplify the analysis, we adopt the following normalisations and definitions:

$$\bar{v} = \frac{v}{v_{th,s}}; \qquad F_s = \frac{v_{th,s}^3 f_s}{n_s}. \tag{2.6}$$

Our normalisation $\bar{v}$ is what Pastukhov (1974) and others refer to as x. We restate the LBO in normalised spherical coordinates to improve clarity,

$$\mathcal{L}(F_s) = \frac{1}{\bar{v}^2}\frac{\partial}{\partial \bar{v}}\bar{v}^3\left(F_s + \frac{1}{2\bar{v}}\frac{\partial F_s}{\partial \bar{v}}\right) + \frac{Z_s}{2\bar{v}^2}\frac{\partial}{\partial \mu}\left(1-\mu^2\right)\frac{\partial F_s}{\partial \mu}. \tag{2.7}$$

We introduce a factor Z_s into the diffusion term to correct for the LBO's approximation of treating the pitch-angle scattering and energy diffusion terms equally. Although for the LBO $Z_s = 1$, an opportunity is left for future work to correct this defect by modifying the coefficient Z_s. The factor of 2 in the pitch-angle scattering in (2.7) comes from the $1/2$ in the $v_{th,s}^2$ term in (2.5). An essential distinction between (2.7) and the collision operators proposed by Pastukhov (1974) and Najmabadi *et al.* (1984) lies in the factors of $\bar{v}$. The collision operators in their work retain the velocity dependence within the Rosenbluth potentials. Below are the collision operators from Pastukhov (1974) and Najmabadi *et al.* (1984),

$$\mathcal{L}_{Najmabadi}(F_s) = \frac{1}{\bar{v}^2}\frac{\partial}{\partial \bar{v}}\left(F_s + \frac{1}{2\bar{v}}\frac{\partial F_s}{\partial \bar{v}}\right) + \frac{1}{\bar{v}^3}\left(Z_{s,N} - \frac{1}{4\bar{v}^2}\right)\frac{\partial}{\partial \mu}\left(1-\mu^2\right)\frac{\partial F_s}{\partial \mu}, \tag{2.8}$$

$$\mathcal{L}_{Pastukhov}(F_s) = \frac{1}{\bar{v}^2}\frac{\partial}{\partial \bar{v}}\left(F_s + \frac{1}{2\bar{v}}\frac{\partial F_s}{\partial \bar{v}}\right) + \frac{1}{\bar{v}^3}\frac{\partial}{\partial \mu}\left(1-\mu^2\right)\frac{\partial F_s}{\partial \mu}, \tag{2.9}$$

where $Z_{s,N}$ is the Z that is used by Najmabadi *et al.* (1984) and N stands for Najmabadi *et al.* (1984), detailed in Appendix B. To compare, the collision operator used by Pastukhov (1974) treats the factor in (2.8) $\left(Z_{s,N} - 1/(4\bar{v}^2)\right)$ as one, although Cohen *et al.* (1986) addresses this limitation in treating the multi-species collisions. Comparing (2.8) and (2.7), we see that the drag and parallel diffusion are missing the $1/\bar{v}^3$ scaling of the more accurate collision operators. However, the pitch angle scattering term is not as bad, scaling as $1/\bar{v}^2$ for the LBO and as $1/\bar{v}^3$ for the more accurate operators.

To simplify the solution, we define a general form for the image problem. We impose that the image sinks start at velocity a, are placed solely outside the loss hyperboloid ($a > \bar{v}_0$ where $\bar{v}_0^2 = z_s e\phi/T_s$) and are isolated to lie along $\mu = \pm 1$ to preserve the symmetry of the problem. As described in figure 1,

$$Q(\bar{v}, \mu) = -\frac{\delta(1-\mu^2)}{4\pi}H(\bar{v}-a)q(\bar{v}), \tag{2.10}$$

where $H()$ is the Heaviside step function and $\delta()$ is the Dirac delta function.

Pastukhov (1974) assume a form for the sinks $q(\bar{v}) = q_0\exp(-\bar{v}^2)$, but the later work by Najmabadi *et al.* (1984) shows that defining $q(\bar{v}) = q_0\exp(-\bar{v}^2)(Z_a -$

Downloaded from https://www.cambridge.org/core. UNIVERSIDAD AUTONOMA METROPOLITANA, on 17 Nov 2026 at 14:11:56, subject to the Cambridge Core terms of use, available at https://www.cambridge.org/core/terms. https://doi.org/10.1017/S0022377825000418

$1/4\bar{v}^2)/\bar{v}^3$ makes the resultant equations simpler to solve with fewer approximations. Najmabadi *et al.* (1984) finds the form of $q(\bar{v})$ by leaving its functional form free during the problem set-up, then choosing a specific form at a later stage to facilitate a solution. Thus, we choose to leave the form of $q(\bar{v})$ arbitrary in (2.10) and will define its form at a later stage.

Without approximation, we can use (2.7) to rewrite (2.2) in the following way:

$$\frac{2e^{\bar{v}^2}}{\bar{v}}\frac{\partial}{\partial e^{\bar{v}^2}}\bar{v}^3\frac{\partial}{\partial e^{\bar{v}^2}}\left(e^{\bar{v}^2}F_s\right)+\frac{Z_s}{2\bar{v}^2}\frac{\partial}{\partial\mu}\left(1-\mu^2\right)\frac{\partial F_s}{\partial\mu}+Q(\bar{v},\mu)=0. \tag{2.11}$$

The inverse chain rule is used to absorb factors of $\bar{v}$ into the derivatives and we also employ the identity $F_s+(1/2\bar{v})\partial_{\bar{v}}F_s=(1/2\bar{v})\exp(-\bar{v}^2)\partial_{\bar{v}}(\exp(\bar{v}^2)F_s)$. Let us define here the variable transformation $z(\bar{v})=\exp(\bar{v}^2)$. We now make a critical approximation: large changes in z cause only small changes in $\bar{v}^2=\ln(z)$, making the derivatives of powers of $\bar{v}$ small. This justifies moving the $\bar{v}^3$ outside the derivative. In more detail, the approximation we make says

$$3\bar{v}^2F_s,\ \bar{v}\frac{\partial F_s}{\partial\bar{v}}\ll\bar{v}^3\frac{\partial F_s}{\partial\bar{v}},\ \bar{v}^3\frac{\partial}{\partial\bar{v}}\left(\frac{1}{2\bar{v}}\frac{\partial F_s}{\partial\bar{v}}\right). \tag{2.12}$$

This is valid since we are only interested in F_s near the loss cone at large velocities, where $\partial F_s/\partial\bar{v}$ is large and $\bar{v}\ll\bar{v}^3$. To simplify further, we define $g(\bar{v},\mu)=\pi^{3/2}\exp(\bar{v}^2)F_s(\bar{v},\mu)$ to factor out the Maxwellian component of the solution. This leads to the new form

$$\left(\frac{\partial^2}{\partial z^2}+\frac{Z_s}{4z^2\ln(z)^2}\frac{\partial}{\partial\mu}\left(1-\mu^2\right)\frac{\partial}{\partial\mu}\right)g_s(\bar{v},\mu)+\frac{\pi^{3/2}}{2z\ln(z)}Q(\bar{v},\mu)=0. \tag{2.13}$$

We aim to make the operator on $g(\bar{v},\mu)$ resemble a cylindrical Laplacian to map this problem to a Poisson problem. For this reason, we must also perform a transformation on the pitch angle scattering component. Consider a general variable transform of the form $\rho(\bar{v},\mu)=h(\bar{v},\mu)\sqrt{1-\mu^2}$. Assuming a large mirror ratio $R\gg1$, we may approximate that near the loss cone $\mu\approx\pm1$. Thus, computing $\partial\rho/\partial\mu$, we neglect $\partial h/\partial\mu$, which would be multiplied by a term $(1-\mu^2)$, which is small. From this, we find $\partial_\mu\approx-(\mu h^2/\rho)\partial_\rho$ and $(1-\mu^2)=\rho^2/h^2$. Under this transformation, $(1-\mu^2)\partial_\mu$ becomes $-\mu\rho\partial_\rho$ without any factors of $h(\bar{v},\mu)$.

Part of the elegance of this method is that we are not limited by the form of $h(\bar{v},\mu)$, as long as z is only a function of $\bar{v}$. For the purpose of an argument, consider an arbitrary transformation $z(\bar{v},\mu)$. If $\partial_\mu z$ were non-zero, we would have to use the chain rule and compute $\partial_\mu\rho(z,\mu)=\partial_z\rho\,\partial_\mu z+\partial_\mu\rho$, thus complicating the procedure. From Najmabadi *et al.* (1984) and here, our variable transformation $z=\exp(\bar{v}^2)$ means that $\partial_z\rho\,\partial_\mu z=0$, making this variable transformation simpler. This insight is perhaps the most pivotal innovation of Najmabadi *et al.* (1984) compared with the variable transformations presented by Pastukhov (1974). Pastukhov (1974) uses a variable transformation $z=\exp(\bar{v}^2)\mu/\sqrt{2\bar{v}^2}$ and $\rho=\exp(\bar{v}^2)\sqrt{1-\mu^2}$, where both variable transformations are functions of $\bar{v}$ and μ. When ultimately satisfying boundary conditions, this leads Pastukhov (1974) to do 'a number of straightforward but rather cumbersome algebraic transformations'. The complications arise due to the prefactors in front of the logarithm in their (17) having a factor of $\bar{v}/\mu$, which comes from the $\mu/\bar{v}$ in their variable transformation for z. In contrast, Najmabadi *et al.* (1984) use the variable transformations $z=\exp(\bar{v}^2)$ and

Downloaded from https://www.cambridge.org/core. UNIVERSIDAD AUTONOMA METROPOLITANA, on 17 Nov 2026 at 14:11:56, subject to the Cambridge Core terms of use, available at https://www.cambridge.org/core/terms. https://doi.org/10.1017/S0022377825000418

$\rho = \sqrt{2\bar{v}^2/(Z_a - 1/4\bar{v}^2)}\exp(\bar{v}^2)\tan\theta$. Notice that, as we have pointed out above, the variable transformation in z does not depend on μ. The equivalent solution is (23) of Najmabadi *et al.* (1984), which is divided by a Maxwellian compared with (17) of Pastukhov (1974). Equation (23) of Najmabadi *et al.* (1984) has a mere constant before the logarithm, making satisfying boundary conditions much simpler.

By setting $h(\bar{v}, \mu)$ to cancel any factor in front of the pitch-angle scattering derivatives, it can be shown that the appropriate variable transformation is

$$\rho(\bar{v}, \mu) = \frac{2z\ln(z)}{\sqrt{Z_s}}\frac{\sqrt{1-\mu^2}}{\mu} = \frac{2z\ln(z)}{\sqrt{Z_s}}\tan\theta. \tag{2.14}$$

As a result, the problem is in the form of a cylindrical Poisson equation,

$$\frac{1}{\rho}\frac{\partial}{\partial\rho}\left(\rho\frac{\partial}{\partial\rho}g_s\right) + \frac{\partial^2 g_s}{\partial^2 z} = \frac{\pi^{3/2}}{2z\ln(z)}\frac{\delta(1-\mu^2)}{4\pi}q(\bar{v})H(\bar{v}-a). \tag{2.15}$$

We can now set the free function $q(\bar{v})$ such that the equation takes an *ad hoc*, easy-to-solve form,

$$\frac{1}{\rho}\frac{\partial}{\partial\rho}\left(\rho\frac{\partial}{\partial\rho}g_s\right) + \frac{\partial^2 g_s}{\partial^2 z} = \frac{\delta(\rho)}{2\pi\rho}4\pi q_0 H(z - z_a). \tag{2.16}$$

On the right-hand side of (2.16), q_0 is equivalent to a constant linear charge density and $z_a = \exp(a^2)$. Although we choose q_0 to be a constant for the sake of having an easy-to-solve problem, it does mean we are sacrificing some detail in the ability to match (2.1) perfectly; however, exact matching is not necessary because the distribution function, as well as losses, decay at higher energies and the majority of particles are lost near the tip of the loss hyperboloid, so that is the region we are most interested in matching. By matching (2.15) and (2.16), we show in Appendix A that the appropriate connection between $q(\bar{v})$ and q_0 is

$$q(\bar{v}) = q_0 \cdot \frac{8}{\sqrt{\pi}}\frac{\mu^2 Z_s}{z\ln(z)}. \tag{2.17}$$

With the new coordinates ρ and z, we transform boundary condition (2.4). In addition, the lower limit of $z = 1$ for $\bar{v} = 0$ is extended to $z = 0$ since $z \equiv \exp(\bar{v}^2) \gg 1$ or set $z' = \exp(\bar{v}^2) - 1 = z(1 + O(\exp(-\bar{v}^2)))$.

$$g_s(\rho, z)|_{z=0} = 1. \tag{2.18}$$

Equation (2.16) with boundary condition (2.18) is solved by Jackson (1999). The equivalent problem in electricity and magnetism terms is having a conducting boundary condition on the $z = 0$ plane held at potential $g_s = 1$ and placing a wire of constant linear charge density q_0 on the z-axis, suspended above the $z = 0$ plane at height $z = z_a$. The standard method of solving this problem is to use the method of images to match the conducting boundary condition. To outline this approach, we use the method of images for the equivalent Poisson problem after previously using the method of images approach to place image sources and sinks in figure 1. This layering of the method of images is why this approach is referred to as the method of images solution for determining loss rates from a magnetic mirror. Only requiring unmapping the equation through stated variable transformations, we find the appropriate distribution function for a magnetic mirror as

Downloaded from https://www.cambridge.org/core. UNIVERSIDAD AUTONOMA METROPOLITANA, on 17 Nov 2026 at 14:11:56, subject to the Cambridge Core terms of use, available at https://www.cambridge.org/core/terms. https://doi.org/10.1017/S0022377825000418

$$g_s(\rho, z) = 1 - q_0 \ln\left(\frac{z_a + z + \sqrt{\rho^2 + (z_a + z)^2}}{z_a - z + \sqrt{\rho^2 + (z_a - z)^2}}\right). \tag{2.19}$$

Mapping this problem back to the magnetic mirror and using that $z \gg 1$ near the loss hyperboloid, we can apply the boundary conditions assigned to this problem in (2.3). Interestingly, this is the only part of the calculation in which information about the magnetic field is used in the solution. We show in Appendix C that for a general variable transformation $z = \exp(\bar{v}^2)$, $\rho = \bar{\rho}(\bar{v}) z \tan\theta$, where $h(\bar{v}, \mu) = \bar{\rho}(\bar{v}) z/\mu$ mentioned earlier, we get

$$q_0 = \left(\ln\left(\frac{w+1}{w-1}\right)\right)^{-1}, \tag{2.20}$$

$$w^2 = 1 + \frac{\bar{\rho}(\bar{v}_0)^2}{2R\bar{v}_0^2} = 1 + \frac{2\bar{v}_0^2}{Z_s R}, \tag{2.21}$$

where $w = \exp(a^2 - \bar{v}_0^2)$. This can be inverted to give $a^2 = \bar{v}_0^2 + \ln(w)$, which determines the edge of the sink region, a, in terms of the tip of the loss region v_0.

Najmabadi *et al.* (1984) adjust the strength of the sinks by examining the difference between the flux of the true loss cone, (2.1), and the approximate loss cone, where (2.19) equals zero. They account for this in their (41*a*) and (41*b*). Their instructions are to evaluate (2.19) along the loss cone one $z_s e\phi/T_s$ above the tip of the loss cone in the limit where $R \gg 1$. This means $\bar{v}^2 = v_0^2 + 1$, $\mu = 1$ and $a \approx v_0$, which leads to $z = \exp(v_0^2 + 1)$ and $\rho = 0$, meaning $g(0, v_0^2 + 1) \approx 1 - q_0 \ln((e+1)/(e-1)) = 1 - 0.77 q_0$. Thus, we modify q_0 by subtracting 0.77, leading to a corrected definition of q_0. Najmabadi *et al.* (1984) determine this to be $0.84 q_0$, but we have not replicated the calculation used to determine their (41*b*),

$$q_0 = \left(\ln\left(\frac{w+1}{w-1}\right) - 0.77\right)^{-1}. \tag{2.22}$$

To calculate this system's confinement time and energy loss rate, we integrate the image sinks over all velocity space, considering the symmetry in gyro- and pitch-angle,

$$\frac{1}{n_s \nu_{sLBO}} \frac{\mathrm{d}n_s}{\mathrm{d}t} = 2\pi \int_0^\infty \bar{v}^2 \mathrm{d}\bar{v} \int_{-1}^1 \mathrm{d}\mu\, Q(\bar{v}, \mu), \tag{2.23}$$

$$\frac{3}{2} \frac{1}{\nu_{sLBO}} \frac{1}{n_s T_s} \frac{\mathrm{d}n_s T_s}{\mathrm{d}t} = 2\pi \int_0^\infty \bar{v}^4 \mathrm{d}\bar{v} \int_{-1}^1 \mathrm{d}\mu\, Q(\bar{v}, \mu). \tag{2.24}$$

Although this appears to be a straightforward integral, there is a subtlety to handling it worth mentioning. Equation (2.23) appears as if it is integrating over half of each delta function on both sides, but it is, in fact, integrating two whole peaks of the delta function across all of velocity space, so $\int_{-1}^1 \delta(1-\mu^2)\mathrm{d}\mu = 1$. Once we account for this intricacy, we arrive at the following forms for confinement time and energy loss rate:

Downloaded from https://www.cambridge.org/core. UNIVERSIDAD AUTONOMA METROPOLITANA, on 17 Nov 2026 at 14:11:56, subject to the Cambridge Core terms of use, available at https://www.cambridge.org/core/terms. https://doi.org/10.1017/S0022377825000418

$$\frac{1}{\tau_c} = \frac{1}{n_s}\frac{\mathrm{d}n_s}{\mathrm{d}t} = -\nu_{sLBO} 2 Z_s \frac{\mathrm{Erfc}(a)}{\ln\left(\frac{w+1}{w-1}\right) - 0.77}, \tag{2.25}$$

$$\frac{1}{E_s}\frac{\mathrm{d}E_s}{\mathrm{d}t} = \frac{1}{n_s T_s}\frac{\mathrm{d}(n_s T_s)}{\mathrm{d}t} = -\nu_{sLBO}\frac{4}{3\sqrt{\pi}} Z_s \frac{e^{-a^2} a + \frac{\sqrt{\pi}}{2}\mathrm{Erfc}(a)}{\ln\left(\frac{w+1}{w-1}\right) - 0.77}. \tag{2.26}$$

Here, τ_c is the confinement time, $E_s = 3/2\, n_s T_s$ is total energy of the system, Erfc() is the complementary error function, $w = \sqrt{1 + 2 z_s e\phi / (T_s Z_s R)}$ and $a = \sqrt{z_s e\phi / T_s + \ln(w)}$.

We proceed to calculate the energy of the particle, but due to collisions, $z_s e\phi / T_s \sim (1/2)\ln(m_i/m_e) \gg 1$. Furthermore, for $R \gg z_s e\phi / T_s Z_s$, $\ln(w)$ is small, giving $a \simeq \sqrt{z_s e\phi / T_s} \gg 1$. The asymptotic expansion for a large argument of the complementary error function is $\mathrm{Erfc}(x) \approx \exp(-x^2)/(\sqrt{\pi} x) \times (1 - 1/2x^2 + 3/4x^4 + \mathcal{O}(1/x^6))$, so τ_c scales as $a \exp(a^2)$. The average energy of lost particles is found by evaluating $E_{s,loss} = (\mathrm{d}E_s/\mathrm{d}t)/(\mathrm{d}n_s/\mathrm{d}t)$,

$$\frac{E_{s,loss}}{T_s} = \frac{1}{2}\left(1 + \frac{2 a e^{-a^2}}{\sqrt{\pi}\mathrm{Erfc}(a)}\right) \tag{2.27}$$

$$\approx a^2 + 1 - \frac{1}{2a^2} + \mathcal{O}(1/a^4). \tag{2.28}$$

It is important to note that (2.25) and subsequent definitions are presented in their un-normalised form. During the un-normalisation process, all quantities are stated in terms of the temperature T_s of the species. This avoids confusion when using a different normalisation procedure for the thermal velocity.

3. Numerical simulations and corrections to (2.20)

We compare our approximate expressions for the loss rates in magnetic mirrors to results obtained using a code based on the work of Ochs *et al.* (2023). The code uses the FEniCS DolfinX Python package to employ the finite element method (FEM) with third-order continuous Galerkin discretisation to solve a general Fokker–Planck model collision operator. The FEM code is meshed over the upper right quadrant of $\bar{v}$, θ space and has a low-energy source of the form $\bar{v}^2 \exp(-\bar{v}^2/\bar{v}_{s0}^2)\theta^2(\pi/2 - \theta)^2$.[1] Here, $\bar{v}$ is normalised velocity and θ is pitch angle. The normalised thermal velocity for the source is evaluated at $\bar{v}_{s0} = 0.2$ to concentrate it at low energy. This source form is chosen to go to zero on the boundaries smoothly (the precise form of the source term has little effect on the results in the asymptotic limit $z_s e\phi / T_e \gg 1$). Zero-flux boundary conditions are used at $\theta = 0$, $\theta = \pi/2$, $v = 0$ and $v = v_{max}$, the maximal velocity extent in the problem. A resolution of $\Delta\theta = \Delta\bar{v} = 0.1$ is chosen, with double resolution near the source and along the loss boundary. The boundary condition on the loss hyperboloid is Dirichlet ($f_s = 0$). The domain is extended $\sqrt{7 + z_s e\phi / T_s}$ past the loss hyperboloid vertex. An example mesh is shown in figure 2 for demonstration. An astute reader will notice that the slope of the loss hyperboloid boundary is not vertical at $\bar{v} = 1$. At the tip of the loss hyperboloid, the code struggles to mesh

[1] There is a typo by Ochs *et al.* (2023), where they miss a negative sign in the exponent.

Downloaded from https://www.cambridge.org/core. UNIVERSIDAD AUTONOMA METROPOLITANA, on 17 Nov 2026 at 14:11:56, subject to the Cambridge Core terms of use, available at https://www.cambridge.org/core/terms. https://doi.org/10.1017/S0022377825000418

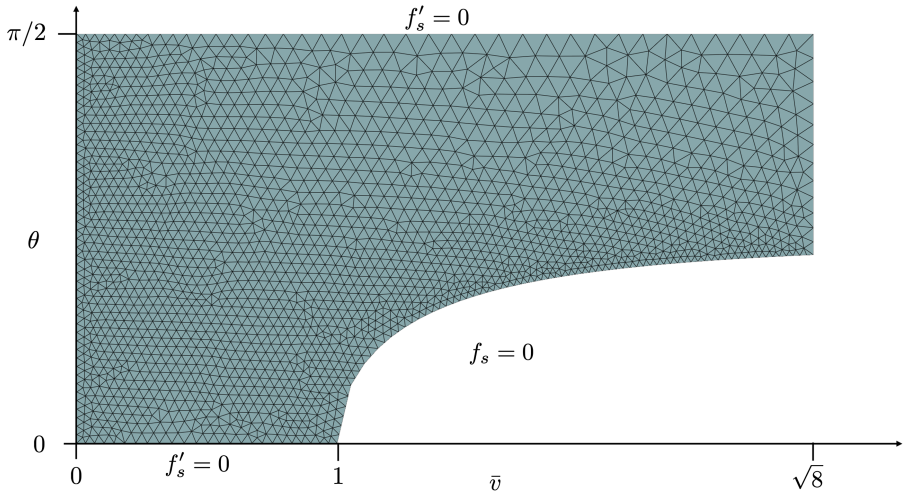


FIGURE 2. An example mesh from the finite element model. Here, $z_s e\phi/T_s = 1$ and $R = 2$ to exaggerate the loss cone.

the boundary because it is purely vertical. A finite step in $\bar{v}$ is taken and the loss boundary is linearly interpolated from the tip of the loss hyperboloid to the first point. This plot was done with a coarser resolution to see the grid. The final results were done at higher resolution confirmed to be adequate with convergence studies. The problem is solved directly using PETSc's linear algebra solvers to find an LU decomposition.

To compare our numerical results to prior computational work, we need to make a key distinction between the collision operator used by our code in reproducing the results from Najmabadi *et al.* (1984) and the operators used in previous work. The results labelled 'FEM Rosenbluth' use a slightly modified version of the collision operator in (2.8), whereas the code used by Cohen *et al.* (1978) and later used by Najmabadi *et al.* (1984) and Fyfe *et al.* (1981) considers a multi-species Fokker–Planck equation derived from nonlinear isotropic Rosenbluth potentials. Naive implementation of (2.8) would violate the assumption that $\bar{v} \gg 1$ because our domain also includes low velocities. The work by Cohen *et al.* (1978) avoided this issue by implementing the full nonlinear Rosenbluth potentials. To address this limitation, we approximate the parallel drag-diffusion frequency in (2.8) by using a Padé approximation of the form $1/\bar{v}^3 \to 1/(1+\bar{v}^3)$, which asymptotically matches the high- and low-velocity Rosenbluth limits. For the pitch angle scattering component, we have a full calculation of the pitch angle scattering rate while considering collisions on a Maxwellian background to keep the problem linear. We consider two cases: a plasma with hydrogen ions and electrons, where either the ions or electrons are electrostatically confined. In both cases, the thermal velocity of electrons is much higher than the thermal velocity of the hydrogen. This results in the following collision operator:

$$\mathcal{L}_{Code}(F_s) = \frac{1}{\bar{v}^2}\frac{\partial}{\partial \bar{v}}\frac{\bar{v}^2}{1+\bar{v}^3}\left(\bar{v}F_s + \frac{1}{2}\frac{\partial F_s}{\partial \bar{v}}\right) + \frac{1}{\bar{v}^3}P(v)\frac{\partial}{\partial \mu}\left(1-\mu^2\right)\frac{\partial F_s}{\partial \mu}. \tag{3.1}$$

For electrostatically confined electrons, $P(v) = (1+\mathcal{R}(v))/2$ ($Z_{s,n} = 1$). For electrostatically confined hydrogen ions, $P(v) = \mathcal{R}(v)/2$ ($Z_{s,n} = 1/2$). In these expressions,

Downloaded from https://www.cambridge.org/core. UNIVERSIDAD AUTONOMA METROPOLITANA, on 17 Nov 2026 at 14:11:56, subject to the Cambridge Core terms of use, available at https://www.cambridge.org/core/terms. https://doi.org/10.1017/S0022377825000418

$\mathcal{R}(v) = 1/(\sqrt{\pi}v)\exp(-v^2) + (1 - 1/2v^2)\mathrm{Erf(v)}$ and Erf is the error function. In contrast, the LBO model is implemented in the code without approximations as (2.7).

To demonstrate convergence, we examine increasing the resolution and the amount of the problem meshed beyond the tip of the loss hyperboloid for $z_s e\phi/T_s = 8$ and $R = 10$. When doubling all resolutions, the resultant loss rate changes by $-0.492\,\%$ for the Dougherty operator and $-1.099\,\%$ for the operator in (3.1). When not changing $\Delta\theta = \Delta\bar{v}$ but quadrupling the resolution near the source and along the loss hyperboloid, the loss rate changes by $-0.493\,\%$ for the Dougherty operator and $-1.001\,\%$ for the operator in (3.1). When increasing the extents of the problem from $\sqrt{7 + z_s e\phi/T_s}$ to $\sqrt{15 + z_s e\phi/T_s}$, the loss rate changes by $-0.06906\,\%$ for the Dougherty operator and $-0.06732\,\%$ for the operator in (3.1). Thus, the code converges within 1 % variation for all collision operators, and this resolution is suitable for this study.

In figure 3, the numerical code is validated by comparing the analytic results presented by Pastukhov (1974) and Najmabadi *et al.* (1984) with corrections noticed by Cohen *et al.* (1978), Najmabadi *et al.* (1984), (2.25) and (2.27), which in turn were validated using other numerical methods. Results in figure 3 agree well with those in many prior works (Najmabadi *et al.* 1984; Cohen *et al.* 1978; Fyfe *et al.* 1981). The confinement time τ_c is normalised to collision frequency for generality. The diamonds are the finite element method numerical results and the dashed lines are the analytic approximations. Although figure 3 shows great agreement with prior work, it has a fair agreement with (2.25). To improve agreement between the code and (2.25), rather than calculating the flux correction coefficient by hand to be 0.77 in (2.22), we can calculate this number numerically. First, let us call this correction coefficient c_0. It can be chosen to minimise error with the finite element code. Equations (2.20), (2.25) and (2.26) are modified to be the following:

$$\frac{1}{\tau_c} = \frac{1}{n_s}\frac{\mathrm{d}n_s}{\mathrm{d}t} = -\nu_{sLBO} 2 Z_s \frac{\mathrm{Erfc}(a)}{\ln\left(\frac{w+1}{w-1}\right) - c_0}, \tag{3.2}$$

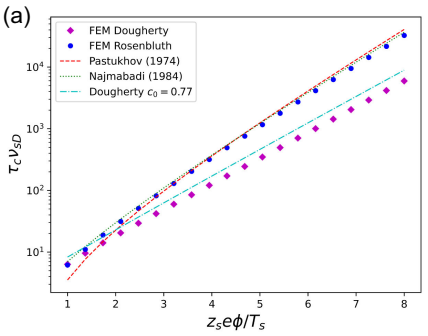
$$\frac{1}{E_s}\frac{\mathrm{d}E_s}{\mathrm{d}t} = \frac{1}{n_s T_s}\frac{\mathrm{d}(n_s T_s)}{\mathrm{d}t} = -\nu_{sLBO}\frac{4}{3\sqrt{\pi}} Z_s \frac{e^{-a^2} a + \frac{\sqrt{\pi}}{2}\mathrm{Erfc}(a)}{\ln\left(\frac{w+1}{w-1}\right) - c_0}. \tag{3.3}$$

In figure 4, we show various curves that describe the error between (3.2) and the finite element code for various values of c_0. This figure shows us that the value of c_0 that minimises error with the finite element code depends on the ambipolar potential and mirror ratio under investigation, although it seems to asymptote to a single value for a sufficiently large mirror ratio and ambipolar potential. In table 1, we list the appropriate correction factor to use for various values of ambipolar potential and mirror ratio that minimise error with the loss rate from the finite element code.

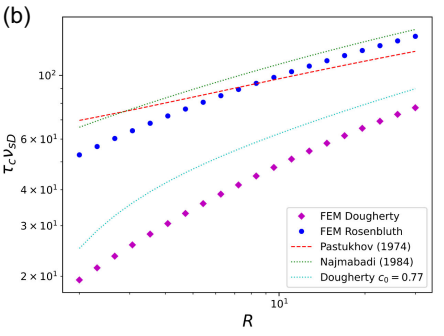
Figure 3 is reconstructed in figure 5 using the correction coefficient c_0 in (3.2) and (3.3). In figure 5(*c*), a choice to not plot the results from Pastukhov (1974) is made due to their close agreements with the results from Najmabadi *et al.* (1984).

In comparing the dependence of the loss rate with ambipolar potential, figure 5(*a*) shows a key difference between the Fokker–Planck form Coulomb operator and the LBO. Using a constant mirror ratio of $R = 10$, the LBO alters the confinement time compared with the Fokker–Planck collision operator used in other studies (Khudik 1997; Najmabadi *et al.* 1984; Pastukhov 1974; Catto & Bernstein 1981; Catto & Li 1985). Particularly, the confinement time of Najmabadi *et al.* (1984)

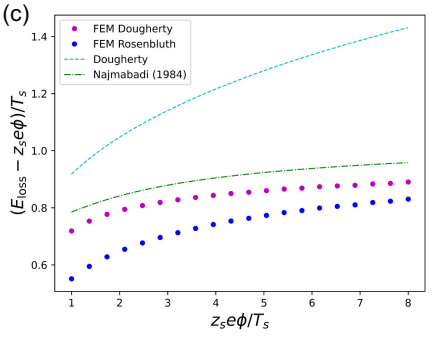
Downloaded from https://www.cambridge.org/core. UNIVERSIDAD AUTONOMA METROPOLITANA, on 17 Nov 2026 at 14:11:56, subject to the Cambridge Core terms of use, available at https://www.cambridge.org/core/terms. https://doi.org/10.1017/S0022377825000418



Confinement time variations with ambipolar potential for $R = 10$ for electrostatically confined electrons ($Z_{s,N} = 1$).



Confinement time variations with mirror ratio for $z_s e\phi/T_s = 3$ for electrostatically confined electrons ($Z_{s,N} = 1$).



Variation of average energy of lost electrons ($Z_{s,N} = 1$) with ambipolar potential for $R = 10$.

FIGURE 3. Normalised particle confinement time $\tau_c \nu_{sLBO}$ from (2.25) and its dependence on ambipolar potential and mirror ratio of the LBO versus Pastukhov (1974), with the correction noticed by Cohen *et al.* (1978) and Najmabadi *et al.* (1984). The y-axis is confinement time, normalised to the collision frequency with $Z_s = 1$ for electrostatically confined electrons.

scales as $a^2 e^{a^2}$, but (3.2) scales as $a e^{a^2}$. This scaling difference makes sense because the LBO overestimates the collision frequency and ignores the collisionality drop-off with velocity.

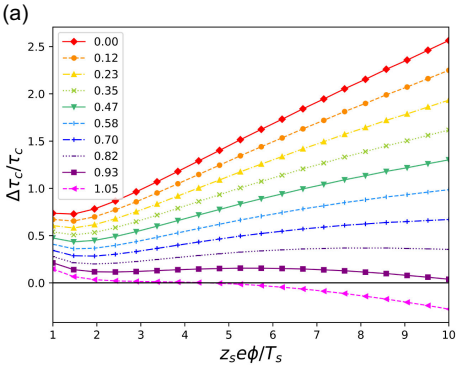
Figures 5(a) and 5(b) compare the variation with potential and mirror ratio of the loss ratios calculated using different collision operators. We see that the LBO model underestimates the confinement time at all potentials and mirror ratios. Even so, the percentage variation of loss rate upon modification of the mirror ratio has similar trends in the finite element code when comparing the LBO model with (3.1). Furthermore, validating the code, each numerical line matches their respective analytic curves well. Figure 5(b) leads us to conclude that there is no significant difference in the dependence of loss rate on mirror ratio when considering LBO collisions.

Figure 5(c) shows that our (2.27) and the numerical approach exhibit similar trends, but are very different in magnitude. It is important to note that figure 5(c)

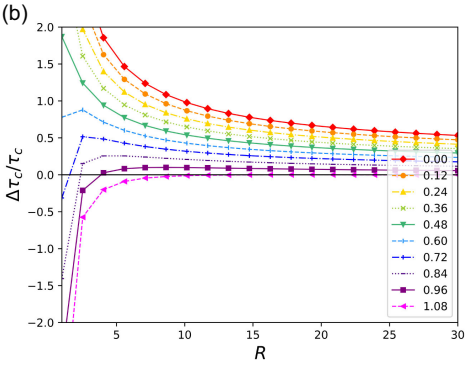
Downloaded from https://www.cambridge.org/core. UNIVERSIDAD AUTONOMA METROPOLITANA, on 17 Nov 2026 at 14:11:56, subject to the Cambridge Core terms of use, available at https://www.cambridge.org/core/terms. https://doi.org/10.1017/S0022377825000418

						R				
$z_s e\phi/T_s$	5	10	15	20	25	30	35	40	45	50
1	1.305	1.310	1.302	1.295	1.288	1.283	1.278	1.274	1.271	1.268
2	1.066	1.094	1.093	1.087	1.080	1.075	1.069	1.065	1.060	1.057
3	1.004	1.066	1.078	1.080	1.077	1.074	1.070	1.066	1.062	1.059
4	0.967	1.057	1.084	1.093	1.095	1.095	1.093	1.091	1.088	1.085
5	0.933	1.044	1.083	1.099	1.107	1.109	1.110	1.109	1.108	1.106
6	0.900	1.027	1.077	1.100	1.112	1.118	1.121	1.122	1.121	1.120
7	0.869	1.007	1.065	1.093	1.109	1.117	1.122	1.125	1.126	1.126
8	0.840	0.987	1.052	1.085	1.104	1.115	1.122	1.126	1.128	1.129
9	0.813	0.968	1.038	1.077	1.099	1.113	1.122	1.128	1.132	1.134
10	0.963	0.948	1.023	1.065	1.090	1.106	1.117	1.124	1.129	1.132

TABLE 1. A table of optimal correction factors c_0 for various values of $z_s e\phi/T_s$ and R to minimise error with the finite element code with $Z_s = 1$.



Confinement time errors with ambipolar potential for $R = 10$.

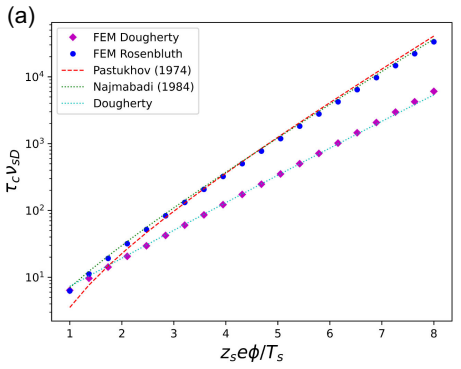


Confinement time errors with mirror ratio for $z_s e\phi/T_s = 3$.

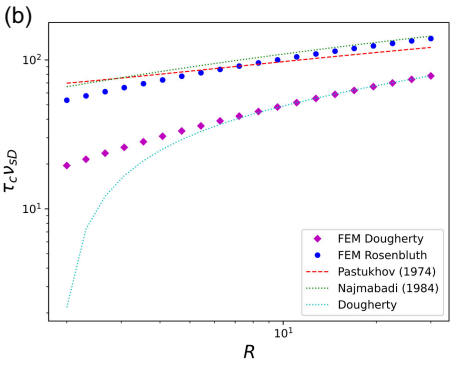
FIGURE 4. Fractional error in the confinement estimates between the numeric code and analytic approximation for electrostatically confined electrons. The legend goes from the top curve to the bottom curve in even steps in the value of c_0.

subtracts the linear component $z_s e\phi/T_s$ to highlight the differences between the different results. Comparing results to prior work, our numerical method produces roughly a 20 % difference with respect to the analytic results from Najmabadi *et al.* (1984), investigated in Appendix B. Although errors of 20 % are large, Najmabadi *et al.* (1984) noticed similar errors, so these results are comparable to prior work. Interestingly, while the analytic results of Najmabadi *et al.* (1984) seem to have a constant 20 % error, the discrepancy between (2.27) and the numerical results grows with $z_s e\phi/T_s$. With the LBO at $c_0 = 0.77$, similar errors of 20 % are observed at low values of $z_s e\phi/T_s$; at large values, the error grows to nearly 50 % at $z_s e\phi/T_s = 8$. The LBO model has an overall higher average loss energy than the model used by Najmabadi *et al.* (1984). This means the losses from LBO collisions are more spread around the loss hyperboloid. In contrast, a more accurate collision operator would

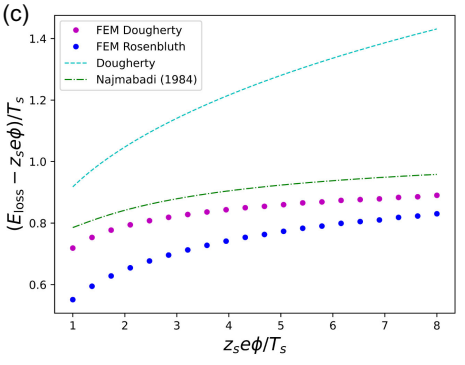
Downloaded from https://www.cambridge.org/core. UNIVERSIDAD AUTONOMA METROPOLITANA, on 17 Nov 2026 at 14:11:56, subject to the Cambridge Core terms of use, available at https://www.cambridge.org/core/terms. https://doi.org/10.1017/S0022377825000418



Confinement time variations with ambipolar potential for $R = 10$, $c_0 = 1.04$, $Z_{s,N} = 1$.



Confinement time variations with mirror ratio for $z_s e\phi/T_s = 3$ and $c_0 = 1.07$, $Z_{s,N} = 1$.



Variation of average energy of lost particles with ambipolar potential for $R = 10$, $c_0 = 1.04$, $Z_{s,N} = 1$.

FIGURE 5. Comparison particle confinement time and average loss energy, and its dependence on ambipolar potential and mirror ratio of the LBO versus Pastukhov (1974) and Najmabadi *et al.* (1984). The y-axis is confinement time or average loss energy subtracted by $z_s e\phi/T_s$, normalised to the collision frequency with $Z_s = 1$ for electrostatically confined electrons.

have losses more concentrated around the tip of the loss hyperboloid. It is worth noting that the correction factor c_0 does not modify (2.27).

4. Discussion

We suggest that codes using an LBO / Dougherty collision operator improve their results by scaling the collision frequency used to obtain the correct mirror confinement time and ambipolar potential. First, one must obtain an accurate estimate of the ambipolar potential of the system. The ambipolar potential may be determined using the analytic results presented by Najmabadi *et al.* (1984) or in a code such as our finite element solver or the one presented by Egedal *et al.* (2022). Using this accurate estimate of ambipolar potential, one can calculate the estimated confinement time using the results from Najmabadi *et al.* (1984), presented in Appendix B. Call this confinement time τ_N. Now that we have calculated the ambipolar potential and confinement time, we may invert (3.2) to determine $\nu_{sLBO} Z_s$, with the appropriate correction coefficient using table 1,

Downloaded from https://www.cambridge.org/core. UNIVERSIDAD AUTONOMA METROPOLITANA, on 17 Nov 2026 at 14:11:56, subject to the Cambridge Core terms of use, available at https://www.cambridge.org/core/terms. https://doi.org/10.1017/S0022377825000418

$$\frac{1}{\nu_{sLBO} Z_s} = 2\tau_{c,N} \left(\ln\left(\frac{w+1}{w-1}\right) - c_0 \right)^{-1} \mathrm{Erfc}(a). \tag{4.1}$$

Here, recall that $w = \sqrt{1 + 2z_s e\phi/(T_s Z_s R)}$ and $a = \sqrt{z_s e\phi/T_s + \ln(w)}$. The simplest approach to achieving the correct results is to scale the collision frequency, setting $Z_s = 1$, which will also have undesirable effects such as modifying multispecies thermal equilibration times (Francisquez *et al.* 2022). Let us define a collision frequency gain constant $\gamma = \nu_{sLBO}/\nu_N$, where ν_N is the collision frequency used in the results of Najmabadi *et al.* (1984). One must scale the collision frequency ν_N by a factor of γ for the loss rate of the system using the LBO to be equal to the system using the operator from Najmabadi *et al.* (1984). Alternatively, one could implement an LBO with a modified diffusion coefficient, including Z_s. Then, one may scale Z_s by a factor of γ instead of collision frequency, which may be preferable depending on the situation. Here, $Z_s \neq 1$ corresponds to an anisotropic collision operator, which can be more accurate but, in some cases, can be numerically more challenging (Sharma & Hammett 2011).

Putting this into practice, we make suggestions of the appropriate scaling factor γ for WHAM and WHAM++. Egedal *et al.* (2022) predicts an ambipolar potential of $z_s e\phi/T_e \simeq 5$ for WHAM and WHAM++. For WHAM, $R = 13.3$ and $\gamma = 0.3030$, and for WHAM++, $R = 10$ and $\gamma = 0.2721$ with $c_0 = 1.05$ and $Z_s = 1$ for both machines. It makes sense that the LBO would need a diminished frequency to match Najmabadi's loss rate because of the $1/v^3$ drop-off in collision frequency at large velocity.

The scrape-off layer of toroidal confinement devices, like tokamaks and stellarators, can exhibit a Pastukhov potential due to the difference in magnetic field strength between the inboard and outboard sides (Majeski *et al.* 2017). The magnetic field magnitude ($|B|$) varies inversely with the distance (R) from the central axis, determining the mirror ratio (R_{out}/R_{in}) of these devices, typically around 2. Additionally, observed potentials are approximately $z_s e\phi/T \sim 2$. This implies these devices have low mirror ratios and a limited potential. In this scenario, figure 5(*a*) aligns reasonably with previous findings by Najmabadi *et al.* (1984). However, Pastukhov (1974) and Najmabadi *et al.* (1984) consider a high mirror ratio and potential limit, making their results inappropriate for toroidal confinement devices. Caution is necessary when applying these equations in regimes approaching the bounds of these limits. The variational method for studying collisional losses not considered here offers an approach suitable for arbitrary mirror ratios and ambipolar potential, making results from Catto & Li (1985) and Khudik (1997) more appropriate.

We note a subtlety in the problem set-up as defined by Pastukhov, Najmabadi and others. It is usually stated that there is a low-energy source of particles to balance the sink at high energy. Standard electron–electron collision operators are energy conserving and the electron–ion collision operator has been approximated by pitch angle scattering, which also conserves energy, so one may wonder where the energy injection comes from. It should be noted that it is not sufficient to add a source to the kinetic equation of the form $S(v) = S_0 \delta(v - v_I)/(4\pi v^2)$ (where S_0 is the source rate in units of particles per second per unit volume), because no choice of the injection velocity v_I can provide enough power for steady state unless v_I is quite large, violating the assumption that the source is at low energy. This is because the source energy per injected particle, $(1/2)mv_I^2$, must be the same in steady state as the average energy per particle lost, which from (2.28) is $E_{loss} \sim z_s e\phi \gg T_e$.

Downloaded from https://www.cambridge.org/core. UNIVERSIDAD AUTONOMA METROPOLITANA, on 17 Nov 2026 at 14:11:56, subject to the Cambridge Core terms of use, available at https://www.cambridge.org/core/terms. https://doi.org/10.1017/S0022377825000418

The resolution to this issue is as follows. In a real mirror machine, the heating of electrons comes from collisions with beam and bulk ions (typically much hotter than the electrons) or RF heating. Collisions and quasilinear RF heating can be roughly modelled here by slightly increasing the velocity diffusion coefficient in the collision operator, i.e. slightly increasing the factor of $v_{th,s}^2$ that appears in the Dougherty–Lenard–Bernstein collision operator (2.5) above the actual thermal velocity squared $\langle v^2\rangle/3$ one would find from the distribution function. Because the mirror confinement time τ_c is much longer than the collision time in the asymptotic regime we are studying, roughly by a factor of $\exp(a^2) \sim \exp(z_s e\phi/T_e) \gg 1$ (neglecting factors of a or a^2 depending on the choice of collision operator), the velocity diffusion coefficient only needs to be increased slightly (the relative change scales as $\exp(-z_s e\phi/T_e) \ll 1$). In numerical codes, this is sometimes implemented via a hidden assumption by not literally using an energy-conserving electron–electron collision operator and instead fixing the value of $v_{th,s}^2$ in the diffusion coefficient as an input parameter. One would find that the actual $\langle v^2\rangle/3$ from the distribution function is slightly less than the input parameter. Some calculations do the same thing by normalising the velocity variable to a fixed parameter, which will turn out to be slightly higher than the actual thermal velocity. Nevertheless again, this is a tiny correction in the asymptotic limit.

5. Conclusion

In summary, this study delves into the critical role that collisions play in governing particle and energy transport within magnetic mirror confinement systems. We use an LBO model to proceed through the method of images calculation to investigate particle and energy confinement. Notably, we address the challenges posed when using a different collision operator compared with prior work.

A pivotal observation emerges when examining the dependence of confinement time on the ambipolar potential, as depicted in figure 5(*a*). The LBO alters the particle confinement time compared with more accurate collision operators used in earlier research (Khudik 1997; Najmabadi *et al.* 1984; Pastukhov 1974; Catto & Bernstein 1981; Catto & Li 1985). Notably, our findings demonstrate that the particle confinement time scales as $a\exp(a^2)$ using the LBO, whereas a more accurate collision operator would yield $a^2\exp(a^2)$, where a^2 is approximately the normalised ambipolar potential, $z_s e\phi/T_e$ (see the inline equations after (2.26)). This scaling discrepancy is attributed to the LBO's disregard for the drop-off in collisionality with velocity. Figure 5(*b*) highlights that despite significantly different loss rates at the same potential, the scaling behaviour with the mirror ratio remains comparable with prior models. Finally, figure 5(*c*) showcases that (3.3) reproduces comparable errors compared with prior work.

To address these findings, we propose a practical modification for codes using an LBO or Dougherty operator to achieve the correct ambipolar potential. This involves estimating the particle loss rate, then calculating the ambipolar potential from a code or predictions from Najmabadi *et al.* (1984). Equation (3.2) can then be employed to determine the appropriate scaling factor for the collision frequency or pitch angle scattering enhancement, ensuring congruence with the electron confinement time. This scaling factor, denoted as γ, depends on various parameters, including the correction factor c_0, which can be interpolated from table 1.

Numerous avenues for extending this research exist. First, the incorporation of anisotropic diffusion coefficients has the potential to alleviate the approximations

Downloaded from https://www.cambridge.org/core. UNIVERSIDAD AUTONOMA METROPOLITANA, on 17 Nov 2026 at 14:11:56, subject to the Cambridge Core terms of use, available at https://www.cambridge.org/core/terms. https://doi.org/10.1017/S0022377825000418

inherent in the LBO operator. This is facilitated by the presence of Z_s in (3.2) and (3.3). Additionally, we have expanded the method of images approach to accommodate alternative forms of the Fokker–Planck coefficients used in the collision operator. Future investigations could explore alternative approximate collision operators using this generalised approach or even take the approximations from Najmabadi *et al.* (1984) to higher order. In addition, the code could be improved by including an improved approximation to the energy diffusion term in (3.1) using the Rosenbluth potentials. Furthermore, future research endeavours might delve into variational techniques, as demonstrated by Catto & Bernstein (1981), Catto & Li (1985) and Khudik (1997), to relax the constraints imposed by large mirror ratios within the method of images. On the computational side, it would be interesting to see how much the results of Francisquez *et al.* (Francisquez et al., 2023) change with rescaling the collision frequency suggested here. Extending the lessons learned here beyond magnetic mirrors, it is worth considering tokamak and stellarator confinement systems. As discussed, toroidal confinement systems exist in the space of low mirror ratios and low potentials, which we studied to be a regime where the loss rate due to LBO collisions has a reasonable agreement with more comprehensive collision operators, and little modification needs to be made. However, this analysis assumed large mirror ratios and large potentials, so more careful analysis must be done using variational techniques for a complete answer.

Acknowledgements

The authors thank Ammar Hakim, Manaure Francisquez and Igor Kaganovich for their helpful discussions culminating in the ideas presented here.

Editor Cary Forest thanks the referees for their advice in evaluating this article.

Funding

This work was supported by Princeton University and the U.S. Department of Energy under contract number DE-AC02-09CH11466. The United States Government retains a non-exclusive, paid-up, irrevocable, world-wide licence to publish or reproduce the published form of this manuscript, or allow others to do so, for United States Government purposes. W.S. was supported by a grant from the Simons Foundation/SFARI (560651, AB) and DoE Grant No. DE-AC02-09CH11466.

Declaration of interests

The authors report no conflict of interest.

Data availability statement

The code and data used to generate the figures in this publication are stored on a private GitHub repository. The source code is available upon request and consultation with the authors.

Appendix A. Convenient choice for the free function $q(\bar{v})$

We will prove (2.17) by first examining the delta function $\delta(1-\mu^2)$ to transform it in terms of ρ. Recalling (2.14), we reorganise this definition to have equality

Downloaded from https://www.cambridge.org/core. UNIVERSIDAD AUTONOMA METROPOLITANA, on 17 Nov 2026 at 14:11:56, subject to the Cambridge Core terms of use, available at https://www.cambridge.org/core/terms. https://doi.org/10.1017/S0022377825000418

$$\frac{Z_s\mu^2\rho^2}{4\bar{v}^4}e^{-2\bar{v}^2} = 1-\mu^2. \tag{A.1}$$

Using the delta function to assert that $\mu = \pm 1$, we can show that the delta function transforms to

$$\delta\left(1-\mu^2\right) = \delta\left(\frac{Z_s\rho^2}{4\bar{v}^4}e^{-2\bar{v}^2}\right) = \delta\left(\rho\right)\frac{2\bar{v}^4}{Z_s\rho}e^{2\bar{v}^2}, \tag{A.2}$$

where we have used $\delta(g(x)) = \delta(x-x_0)/|g'(x_0)|$ with x_0 satisfying $g(x_0) = 0$. Transforming $Q(\bar{v}, \mu)$, we then get

$$\frac{\pi^{3/2}}{2z\ln(z)}\frac{\delta(1-\mu^2)}{4\pi}H(\bar{v}-a)q(\bar{v}) = \frac{\delta\left(\rho\right)}{2\pi\rho}H(z-z_a)4\pi\left(\frac{z\ln(z)\sqrt{\pi}}{8Z_s}q(\bar{v})\right), \tag{A.3}$$

where we have grouped terms to get it in the form of (2.16). We find (2.17) by setting $q(\bar{v})$ to cancel out this functional dependence and leave within it some arbitrary functionality $\bar{q}$. This follows the approach set forth by Najmabadi *et al.* (1984), where they set this to a constant for simplicity.

Appendix B. Investigation into the correction factor of Najmabadi *et al.* (1984)

The notation used in this paper is very similar to the notation used by Najmabadi *et al.* (1984). For clarity, let us define some of the key differences in notation, which will be used exclusively in this appendix section. For the collision operator used by Najmabadi *et al.* (1984), they define the appropriate collision frequency and anisotropic diffusion coefficients considering multispecies collisions:

$$\nu_e \equiv \frac{4\pi}{m_e^2 v_{th,e}^3}\left(\frac{e^2}{4\pi\epsilon_0}\right)^2 n_e\lambda_{ee}, \qquad Z_{e,N} \equiv \frac{1}{2}\left(1+\frac{\sum_j n_j z_j^2\lambda_{ej}}{n_e\lambda_{ee}}\right), \tag{B.1}$$

$$\nu_i \equiv 4\pi\left(\frac{e^2}{4\pi\epsilon_0}\right)^2\sum_j\frac{n_j z_i^2 z_j^2\lambda_{ij}}{m_i m_j v_{th,i}^2}\frac{T_j}{T_i}, \quad Z_{i,N} \equiv \frac{1}{2}\frac{\sum_j n_j z_j^2\lambda_{ij}}{\sum_j n_j z_j^2\lambda_{ij}(T_j/T_i)(m_i/m_j)}. \tag{B.2}$$

where $\sum_j$ is a summation over ions only, $v_{th,s} = \sqrt{2T_s/m_s}$ e is the electronic charge, z_s is the atomic number of species s, λ_{ab} is the Coulomb logarithm and ϵ_0 is the dielectric constant.

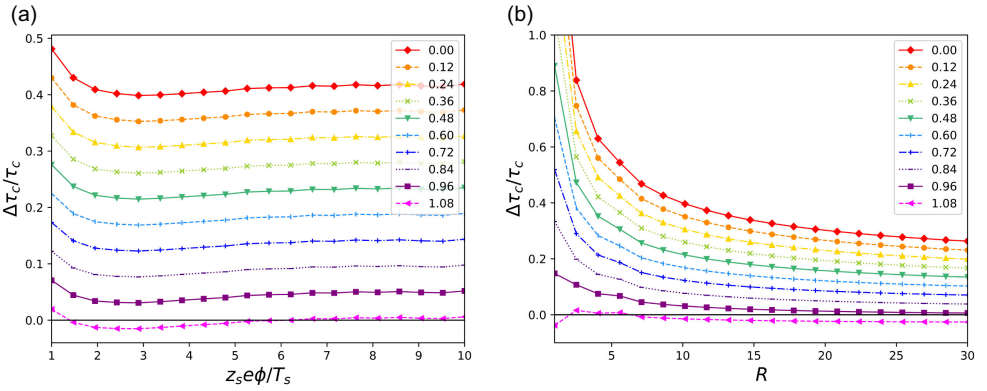
We restate the main finding from Najmabadi *et al.* (1984). They found that the confinement time scales as

$$\frac{1}{\tau_{c,N}} = \nu_s\frac{4}{\sqrt{\pi}}\frac{\exp(-a^2)}{a^2}\frac{\left(Z_{s,N}+1/4\right)a^2\exp(a^2)E_1(a^2)-1/4}{\ln\left(\frac{w+1}{w-1}\right)-c_N}. \tag{B.3}$$

Here, $w = \sqrt{1+2/\left(R(Z_s-T_s/4z_s e\phi)\right)}$ and $a^2 = z_s e\phi/T_s + \ln(w)$, $E_1(x) = \int_x^\infty \mathrm{d}t\exp(-t)/t$ is the exponential integral, c_N is a correction coefficient, and the subscript N stands for Najmabadi *et al.* (1984).[2]

[2]There is a typo in the second statement of w by Najmabadi *et al.* (1984) near (42) which should have a square root, noticed by Ochs *et al.* (2023).

Downloaded from https://www.cambridge.org/core. UNIVERSIDAD AUTONOMA METROPOLITANA, on 17 Nov 2026 at 14:11:56, subject to the Cambridge Core terms of use, available at https://www.cambridge.org/core/terms. https://doi.org/10.1017/S0022377825000418



Confinement time errors with ambipolar potential for $R = 10$.

Confinement time errors with mirror ratio for $z_s e\phi/T_s = 3$.

FIGURE 6. Fractional error in the confinement estimates between (B.3) and the finite element code for electrostatically confined electrons. The legend goes from the top curve to the bottom curve in even steps in the value of c_0.

Najmabadi *et al.* (1984) determine $c_N = 0.84$, although we have not replicated the calculation used to determine this. In (B.3), it is essential to notice that the correction coefficient does change the asymptotic convergence of the problem. The authors claim that this convergence is enhanced from $\mathcal{O}(1/x_a^2)$ to $\mathcal{O}(\exp(-x_z^2))$, but adding this 0.84 changes to where q_0 asymptotes, so it does more than yield faster convergence; it changes the convergence entirely. This is showcased in figure 6, where it is clear that the error asymptotes to a constant level, which depends strongly on c_N. Without using this correction factor, the error saturates to approximately 40 % compared with the numerical code, which is quite large and not converging. With $c_N = 0.84$, (B.3) has a roughly 10 % error with the finite element code, whereas Najmabadi *et al.* (1984) report errors of ± 7 %. Their expression for q_0 is the same as with the LBO, $\ln(w + 1/w - 1)$, but their w takes the form for large $z_s e\phi/T_s$ of $w = \sqrt{1 + 1/RZ_s}$. Therefore, q_0 asymptotes at large R to $\ln(1 + 4RZ_s)$. This number is not large and is comparable to the coefficient of 0.84 they find.

We do not expect the same coefficient that Najmabadi *et al.* (1984) find because our approximate distribution function takes a different form, using different powers of velocity. It is worth noting that w asymptotes very differently with the LBO than with the Coulomb operator, which leads to these differences. Since $w = \sqrt{1 + 2z_s e\phi/(T_s Z_s R)}$, we order $z_s e\phi/T_s < Z_s R$. Then, we get $q_0 = \ln(1 + 2Z_s RT_s/(z_s e\phi))$, which is also not large and is affected by the convergence factor. The dependence of this q_0 on $z_s e\phi/T_s$ affects the convergence, making it more complex to determine the appropriate asymptotic behaviour.

Instead, we opt to apply the same numerical technique employed in § 3. By calculating the value of c_N that minimises the error between our finite element code, we determine the appropriate value of c_N. Table 2 has the appropriate correction coefficients for a pure hydrogen plasma ($Z_s = 1/2$) and table 3 has the correction coefficients for electrons with a hydrogen background ($Z_s = 1$). Intriguingly, this coefficient depends on the pitch angle scattering rate Z_s. It is clear from these tables that Najmabadi *et al.* (1984) calculated this as a constant, but it has a much more complicated dependency in matching the finite element code. It is essential to

Downloaded from https://www.cambridge.org/core. UNIVERSIDAD AUTONOMA METROPOLITANA, on 17 Nov 2026 at 14:11:56, subject to the Cambridge Core terms of use, available at https://www.cambridge.org/core/terms. https://doi.org/10.1017/S0022377825000418

						R				
$z_s e\phi/T_s$	5	10	15	20	25	30	35	40	45	50
1	0.876	0.860	0.777	0.770	0.691	0.702	0.680	0.653	0.649	0.679
2	1.056	1.030	1.009	0.967	0.965	0.965	0.942	0.940	0.928	0.924
3	1.095	1.082	1.062	1.046	1.034	1.021	1.016	1.008	0.996	1.017
4	1.114	1.107	1.091	1.078	1.067	1.058	1.051	1.044	1.039	1.035
5	1.126	1.121	1.106	1.093	1.083	1.075	1.068	1.062	1.057	1.053
6	1.134	1.131	1.117	1.104	1.095	1.087	1.080	1.075	1.070	1.064
7	1.136	1.132	1.117	1.104	1.095	1.086	1.080	1.073	1.068	1.066
8	1.138	1.133	1.119	1.106	1.098	1.089	1.081	1.076	1.070	1.068
9	1.142	1.140	1.127	1.117	1.103	1.095	1.088	1.085	1.083	1.079
10	1.142	1.141	1.123	1.118	1.106	1.093	1.084	1.079	1.079	1.091

TABLE 2. A table of optimal correction factors c_N for various values of $z_s e\phi/T_s$ and R to minimise error with the finite element code for hydrogen $Z_s = 1/2$.

						R				
$z_s e\phi/T_s$	5	10	15	20	25	30	35	40	45	50
1	1.183	1.125	1.093	1.068	1.052	1.040	1.031	1.023	1.017	1.013
2	1.093	1.046	1.018	0.999	0.986	0.976	0.968	0.963	0.958	0.953
3	1.081	1.042	1.018	1.002	0.991	0.983	0.976	0.971	0.966	0.963
4	1.090	1.056	1.035	1.020	1.010	1.003	0.997	0.992	0.988	0.984
5	1.101	1.069	1.048	1.034	1.026	1.018	1.012	1.008	1.004	1.001
6	1.112	1.083	1.062	1.048	1.041	1.033	1.028	1.023	1.020	1.014
7	1.115	1.084	1.063	1.049	1.042	1.035	1.029	1.024	1.020	1.020
8	1.119	1.088	1.067	1.054	1.046	1.038	1.033	1.030	1.024	1.023
9	1.127	1.097	1.078	1.066	1.054	1.050	1.043	1.042	1.041	1.035
10	1.124	1.096	1.075	1.071	1.056	1.052	1.035	1.032	1.044	1.033

TABLE 3. A table of optimal correction factors c_N for various values of $z_s e\phi/T_s$ and R to minimise error with the finite element code for electrons $Z_s = 1$.

mention that the collision operator used by the finite element code is approximate, especially at low velocities, which impacts the results at low values of $z_s e\phi/T_s$. However, it is intriguing that this coefficient does not asymptote to a constant at large values of R or $z_s e\phi/T_s$, which they suggest should occur. Furthermore, using this coefficient table effectively provides a much better estimation of the results from the finite element code than the original work. Nonetheless, all figures in the rest of the paper are produced with $c_N = 0.84$ as it still is a reasonable estimate.

Appendix C. Loss cone boundary conditions

From (2.3), we have two boundary conditions to fix q_0 and a. Recall $g(\bar{v}, \mu) = \pi^{3/2} \exp(\bar{v}^2) F_s(\bar{v}, \mu)$ and hence,

$$g(\rho, z)|_{z=z_0, \rho=0} = 0. \tag{C.1}$$

This is straightforward to apply from (2.19),

Downloaded from https://www.cambridge.org/core. UNIVERSIDAD AUTONOMA METROPOLITANA, on 17 Nov 2026 at 14:11:56, subject to the Cambridge Core terms of use, available at https://www.cambridge.org/core/terms. https://doi.org/10.1017/S0022377825000418

$$q_0 = \left(\ln\left(\frac{w+1}{w-1}\right)\right)^{-1}, \tag{C.2}$$

where $w = \exp(a^2 - \bar{v}_0^2)$. Equation (C.2) can be rewritten as $w = \coth(1/2q_0)$.

Now, we will expand the second condition in (2.3), that the curvature of the contour where our fitted distribution function is zero near the loss cone matches the curvature of the true loss cone. For the sake of generality, we will refer to a variable transformation where the velocity transformation is the same, $z = \exp(\bar{v}^2)$, but the pitch angle transformation is in the general form of $\rho = \bar{\rho}(\bar{v})z\sqrt{1-\mu^2}/\mu = \bar{\rho}(\bar{v})z\tan\theta \approx \bar{\rho}(\bar{v})z\theta$, where we have isolated the separate pitch angle and velocity dependence. With this form,

$$\partial_{\bar{v}} F(\bar{v}, \mu) = \partial_{\bar{v}}\left(\frac{g(\rho, z)}{\pi^{3/2}z}\right) = \frac{1}{\pi^{3/2}z}\partial_{\bar{v}} g(\rho, z) \tag{C.3}$$

and

$$\partial_{\mu} F(\bar{v}, \mu) = \partial_{\mu}\left(\frac{g(\rho, z)}{\pi^{3/2}z}\right) = \frac{1}{\pi^{3/2}z}\partial_{\mu} g(\rho, z). \tag{C.4}$$

So from changing distribution function from $F_s(\bar{v}, \mu)$ to $g(\rho, z)$,

$$\left.\frac{\partial_{\bar{v}} g}{\partial_{\mu} g}\right|_{z=z_0, \rho=0} = \frac{1}{R\bar{v}_0}, \tag{C.5}$$

where we have used $g(0, z_0) = 0$. Continuing, we must expand the partial derivatives in $\bar{v}$ and μ into their respective derivatives in terms of ρ and z using the chain rule,

$$\partial_{\bar{v}} g(\rho, z) = \frac{\partial g}{\partial \rho}\frac{\partial \rho}{\partial \bar{v}} + \frac{\partial g}{\partial z}\frac{\partial z}{\partial \bar{v}} = \frac{\partial g}{\partial \rho}\rho\left(2\bar{v} + \frac{\bar{\rho}'}{\bar{\rho}}\right) + \frac{\partial g}{\partial z}2\bar{v}z, \tag{C.6}$$

$$\partial_{\mu} g = \frac{\partial g}{\partial \rho}\frac{\partial \rho}{\partial \mu} = \frac{\partial g}{\partial \rho}\frac{\partial \rho}{\partial(\cos\theta)} \approx \frac{\partial g}{\partial \rho}\frac{\partial \rho}{-\theta\,\partial\theta} = \frac{\partial g}{\partial \rho}\frac{\bar{\rho}(\bar{v})z}{-\theta} = -\frac{\partial g}{\partial \rho}\frac{\rho}{\theta^2}. \tag{C.7}$$

One of the beautiful aspects of this derivation is that this specific choice of variables results in a simple form of the derivative in μ. Furthermore, it can be shown that the derivatives of (2.19) are

$$\left.\frac{\partial g}{\partial z}\right|_{z=z_0, \rho=0} = -\frac{2q_0 w}{z_0(w^2-1)}, \tag{C.8}$$

$$\left.\frac{\partial g}{\partial \rho}\right|_{z=z_0, \rho\ll 1} = -\frac{q_0\rho}{2z_0^2}\left[\frac{1}{(w+1)^2} - \frac{1}{(w-1)^2}\right]. \tag{C.9}$$

Now, we can plug it all back in together,

$$\frac{1}{R\bar{v}_0} = \left.\frac{\frac{\partial g}{\partial \rho}\rho\left(2\bar{v} + \frac{\bar{\rho}'}{\bar{\rho}}\right) + \frac{\partial g}{\partial z}2\bar{v}z}{\frac{q_0}{2z_0^2}\left[\frac{1}{(w+1)^2} - \frac{1}{(w-1)^2}\right]\frac{\rho^2}{\theta^2}}\right|_{z=z_0, \rho\to 0}. \tag{C.10}$$

Downloaded from https://www.cambridge.org/core. UNIVERSIDAD AUTONOMA METROPOLITANA, on 17 Nov 2026 at 14:11:56, subject to the Cambridge Core terms of use, available at https://www.cambridge.org/core/terms. https://doi.org/10.1017/S0022377825000418

Next, we notice that $\rho \to 0$ and $\partial_\rho g \propto \rho$, so the $\partial_\rho g$ term in the numerator is negligible. We also see that $\rho^2/\theta^2 = \bar{\rho}^2 z_0^2$ for $z = z_0$ and $\theta \ll 1$, giving

$$\frac{1}{R\bar{v}_0} = \frac{2\bar{v}_0}{\bar{\rho}(\bar{v}_0)^2}\left(w^2 - 1\right). \tag{C.11}$$

Solving for w we find (2.21). For the collision operator of Najmabadi *et al.* (1984), $\bar{\rho}(\bar{v})^2 = 2\bar{v}^2/(Z_s - 1/4\bar{v}^2)$, so their equivalent expression would be

$$w^2 = 1 + \frac{1}{R(Z_s - 1/4\bar{v}_0^2)}, \tag{C.12}$$

which agrees with the results of Najmabadi *et al.* (1984). For Dougherty, we use $\bar{\rho}(\bar{v})^2 = 4\bar{v}^4/Z_s$, so the matching condition becomes the second equality in (2.21).

REFERENCES

BAGRYANSKY, P.A. *et al.* 2011 Confinement of hot ion plasma with β= 0.6 in the gas dynamic trap. *Fusion Sci. Technol.* **59** (1T), 31–35.

BAGRYANSKY, P.A., SHALASHOV, A.G., GOSPODCHIKOV, E.D., LIZUNOV, A.A., MAXIMOV, V.V., PRIKHODKO, V.V., SOLDATKINA, E.I., SOLOMAKHIN, A.L. & YAKOVLEV, D.V. 2015 Threefold increase of the bulk electron temperature of plasma discharges in a magnetic mirror device. *Phys. Rev. Lett.* **114**, 205001.

BEKLEMISHEV, A.D. 2017 Tail-waving system for active feedback stabilization of flute modes in open traps. *Fusion Sci. Technol.* **59** (1T), 90–93.

BEKLEMISHEV, A.D., BAGRYANSKY, P.A., CHASCHIN, M.S. & SOLDATKINA, E.I. 2010 Vortex confinement of plasmas in symmetric mirror traps. *Fusion Sci. Technol.* **57** (4), 351–360.

BERK, H.L. & CHEN, C.Y. 1988 Dissipative trapped particle modes in tandem mirrors. *Phys. Fluids* **31** (1), 137–148.

CATTO, P.J. & BERNSTEIN, I.B. 1981 Collisional end losses from conventional and tandem mirrors. *Phys. Fluids* **24** (10), 1900–1905.

CATTO, P. J. & LI, X.Z. 1985 Particle loss rates from electrostatic wells of arbitrary mirror ratios. *Phys. Fluids* **28** (1), 352–357.

CELEBRE, G., SERVIDIO, S. & VALENTINI, F. 2023 Phase space dynamics of unmagnetized plasmas: collisionless and collisional regimes. *Phys. Plasmas* **30** (9), 092304.

CHERNIN, D.P. & ROSENBLUTH, M.N. 1978 Ion losses from end-stoppered mirror trap. *Nucl. Fusion* **18** (1), 47.

COHEN, B.I., FREIS, R.P. & NEWCOMB, W.A. 1986 Interchange, rotational, and ballooning stability of long-thin axisymmetric systems with finite-orbit effects. *Phys. Fluids* **29** (5), 1558–1577.

COHEN, R.H., RENSINK, M.E., CUTLER, T.A. & MIRIN, A.A. 1978 Collisional loss of electrostatically confined species in a magnetic mirror. *Nucl. Fusion* **18** (9), 1229–1243.

DOUGHERTY, J.P. 1964 Model Fokker-Planck equation for a plasma and its solution. *Phys. Fluids* **7** (11), 1788–1799.

EGEDAL, J., ENDRIZZI, D., FOREST, C.B. & FOWLER, T.K. 2022 Fusion by beam ions in a low collisionality, high mirror ratio magnetic mirror. *Nucl. Fusion* **62** (12), 126053.

ENDRIZZI, D. *et al.* 2023 Physics basis for the Wisconsin HTS Axisymmetric Mirror (WHAM). *J. Plasma Phys.* **89** (5), 975890501.

FOWLER, T.K., MOIR, R.W. & SIMONEN, T.C. 2017 A new simpler way to obtain high fusion power gain in tandem mirrors. *Nucl. Fusion* **57** (5), 056014.

FRANCISQUEZ, M., BERNARD, T.N., MANDELL, N.R., HAMMETT, G.W. & HAKIM, A. 2020 Conservative discontinuous Galerkin scheme of a gyro-averaged Dougherty collision operator. *Nucl. Fusion* **60** (9), 096021.

FRANCISQUEZ, M., JUNO, J., HAKIM, A., HAMMETT, G.W. & ERNST, D.R. 2022 Improved multispecies Dougherty collisions. *J. Plasma Phys.* **88** (3), 905880303.

Downloaded from https://www.cambridge.org/core. UNIVERSIDAD AUTONOMA METROPOLITANA, on 17 Nov 2026 at 14:11:56, subject to the Cambridge Core terms of use, available at https://www.cambridge.org/core/terms. https://doi.org/10.1017/S0022377825000418

FRANCISQUEZ, M., ROSEN, M.H., MANDELL, N.R., HAKIM, A., FOREST, C.B. & HAMMETT, G.W. 2023 Toward continuum gyrokinetic study of high-field mirrors. *Phys. Plasmas* **30** (10), 102504.

FREI, B.J., HOFFMANN, A.C.D. & RICCI, P. 2022 Local gyrokinetic collisional theory of the ion-temperature gradient mode. *J. Plasma Phys.* **88** (3), 905880304.

FYFE, D., WEISER, A., BERNSTEIN, I., EISENSTAT, S. & SCHULTZ, M. 1981 A finite element solution of a reduced Fokker-Planck equation. *J. Comput. Phys.* **42** (2), 327–336.

GRANDGIRARD, V. *et al.* 2016 A 5D gyrokinetic full- f global semi-Lagrangian code for flux-driven ion turbulence simulations. *Comput. Phys. Commun.* **207**, 35–68.

HAKIM, A., FRANCISQUEZ, M., JUNO, J. & HAMMETT, G.W. 2020 Conservative discontinuous Galerkin schemes for nonlinear Dougherty–Fokker–Planck collision operators. *J. Plasma Phys.* **86** (4), 905860403.

HATCH, D.R., JENKO, F., BAÑÓN NAVARRO, A. & BRATANOV, V. 2013 Transition between saturation regimes of gyrokinetic turbulence. *Phys. Rev. Lett.* **111** (17), 175001.

HIRSHMAN, S.P. & SIGMAR, D.J. 1976 Approximate Fokker–Planck collision operator for transport theory applications. *Phys. Fluids* **19** (10), 1532–1540.

HOFFMANN, A.C.D., FREI, B.J. & RICCI, P. 2023 Gyrokinetic simulations of plasma turbulence in a Z-pinch using a moment-based approach and advanced collision operators. *J. Plasma Phys.* **89** (2), 905890214.

JACKSON, J.D. 1999 *Classical Electrodynamics*. 3rd edition. John Wiley & Sons.

KHUDIK, V.N. 1997 Longitudinal losses of electrostatically confined particles from a mirror device with arbitrary mirror ratio. *Nucl. Fusion* **37** (2), 189–198.

KNYAZEV, A.R., DORF, M. & KRASHENINNIKOV, S.I. 2023 Implementation and verification of a model linearized multi-species collision operator in the cogent code. *Comput. Phys. Commun.* **291**, 108829.

LENARD, A. & BERNSTEIN, I.B. 1958 Plasma oscillations with diffusion in velocity space. *Phys. Rev.* **112** (5), 1456–1459.

LOUREIRO, N.F., DORLAND, W., FAZENDEIRO, L., KANEKAR, A., MALLET, A., VILELAS, M.S. & ZOCCO, A. 2016 Viriato: a Fourier–Hermite spectral code for strongly magnetized fluid–kinetic plasma dynamics. *Comput. Phys. Commun.* **206**, 45–63.

MAJESKI, R. *et al.* 2017 Compatibility of lithium plasma-facing surfaces with high edge temperatures in the Lithium Tokamak Experiment. *Phys. Plasmas* **24** (5), 056110.

MANDELL, N.R., DORLAND, W., ABEL, I., GAUR, R., KIM, P., MARTIN, M. & QIAN, T. 2022 GX: a GPU-native gyrokinetic turbulence code for tokamak and stellarator design. *Arxiv*, 2209.06731, https://arxiv.org/abs/2209.06731

NAJMABADI, F., CONN, R.W. & COHEN, R.H. 1984 Collisional end loss of electrostatically confined particles in a magnetic mirror field. *Nucl. Fusion* **24** (1), 75–84.

OCHS, I.E., MUNIROV, V.R. & FISCH, N.J. 2023 Confinement time and ambipolar potential in a relativistic mirror-confined plasma. *Phys. Plasmas* **30** (5), 052508.

PARKER, J.T. & DELLAR, P.J. 2015 Fourier–Hermite spectral representation for the Vlasov–Poisson system in the weakly collisional limit. *J. Plasma Phys.* **81** (2), 305810203.

PASTUKHOV, V.P. 1974 Collisional losses of electrons from an adiabatic trap in a plasma with a positive potential. *Nucl. Fusion* **14** (1), 3–6.

PERRONE, L.M., JORGE, R. & RICCI, P. 2020 Four-dimensional drift-kinetic model for scrape-off layer plasmas. *Phys. Plasmas* **27** (11), 112502.

PEZZI, O., CAMPOREALE, E. & VALENTINI, F. 2016 Collisional effects on the numerical recurrence in Vlasov-Poisson simulations. *Phys. Plasmas* **23** (2), 022103.

POST, R.F. & ROSENBLUTH, M.N. 1966 Electrostatic instabilities in finite mirror-confined plasmas. *Phys. Fluids* **9** (4), 730–749.

ROSENBLUTH, M.N., MACDONALD, W.M. & JUDD, D.L. 1957 Fokker-Planck equation for an inverse-square force. *Phys. Rev.* **107** (1), 1–6.

RYUTOV, D.D., BERK, H.L., COHEN, B.I., MOLVIK, A.W. & SIMONEN, T.C. 2011 Magneto-hydrodynamically stable axisymmetric mirrors. *Phys. Plasmas* **18** (9), 092301.

SHARMA, P. & HAMMETT, G.W. 2011 A fast semi-implicit method for anisotropic diffusion. *J. Comput. Phys.* **230** (12), 4899–4909.

Downloaded from https://www.cambridge.org/core. UNIVERSIDAD AUTONOMA METROPOLITANA, on 17 Nov 2026 at 14:11:56, subject to the Cambridge Core terms of use , available at https://www.cambridge.org/core/terms. https://doi.org/10.1017/S0022377825000418

TAITANO, W.T., CHACÓN, L., SIMAKOV, A.N. & MOLVIG, K. 2015 A mass, momentum, and energy conserving, fully implicit, scalable algorithm for the multi-dimensional, multi-species Rosenbluth–Fokker–Planck equation. *J. Comput. Phys.* **297**, 357–380.

ULBL, P., BODY, T., ZHOLOBENKO, W., STEGMEIR, A., PFENNIG, J. & JENKO, F. 2023 Influence of collisions on the validation of global gyrokinetic simulations in the edge and scrape-off layer of TCV. *Phys. Plasmas* **30** (5), 052507.

ULBL, P., MICHELS, D. & JENKO, F. 2022 Implementation and verification of a conservative, multi-species, gyro-averaged, full- f, Lenard-Bernstein /Dougherty collision operator in the gyrokinetic code GENE-X. *Contrib. Plasma Phys.* **62** (5-6), e202100180.

WHITE, R., HASSAM, A. & BRIZARD, A. 2018 Centrifugal particle confinement in mirror geometry. *Phys. Plasmas* **25** (1), 012514.

YE, B., HU, J., SHU, C.-W. & ZHONG, X. 2024 Energy-conserving discontinuous Galerkin methods for the Vlasov-Ampère system with Dougherty-Fokker-Planck collision operator. *J. Comput. Phys.* **514**, 113219.

Downloaded from https://www.cambridge.org/core. UNIVERSIDAD AUTONOMA METROPOLITANA, on 17 Nov 2026 at 14:11:56, subject to the Cambridge Core terms of use , available at https://www.cambridge.org/core/terms. https://doi.org/10.1017/S0022377825000418